Biogeosciences Discuss., 8, 7007–7032, 2011
www.biogeosciences-discuss.net/8/7007/2011/
doi:10.5194/bgd-8-7007-2011

Biogeosciences Discussions

Will open ocean oxygen stress intensify under climate change?

A. Gnanadesikan[1,2], J. P. Dunne[2], and J. John[2]

[1]Department of Earth and Planetary Sciences, Johns Hopkins University, 3400 N. Charles St., Baltimore, MD, USA
[2]NOAA Geophysical Fluid Dynamics Laboratory, Forrestal Campus, Princeton, NJ, USA

Received: 1 July 2011 – Accepted: 11 July 2011 – Published: 15 July 2011

Correspondence to: A. Gnanadesikan (gnanades@jhu.edu)

Published by Copernicus Publications on behalf of the European Geosciences Union.

Abstract

Global warming is expected to reduce oxygen solubility and vertical exchange in the ocean, changes which would be expected to result in an increase in the volume of hypoxic waters. A simulation made with a full earth system model with dynamical atmosphere, ocean, sea ice and biogeochemical cycling shows that this holds true if the condition for hypoxia is set relatively high. However, the volume of the most hypoxic waters does not increase under global warming, as these waters actually become more oxygenated. We show that the rise in oxygen is associated with a drop in ventilation time. A term-by-term analysis within the least oxygenated waters shows an increased supply of oxygen due to lateral diffusion. compensating an increase in remineralization within these highly hypoxic waters. This lateral diffusive flux is the result of an increase of ventilation along the Chilean coast, as a drying of the region under global warming opens up a region of wintertime convection in our model.

1 Introduction

Ten percent of today's ocean volume is characterized by low level of dissolved oxygen similar to those found in the well-known "dead zones" in the Gulf of Mexico with 35 % of global surface waters overlying at least some of this "hypoxia" ($O_2 < 88\,\mu M \sim 2\,ml\,l^{-1}$) (Garcia et al., 2010). Under global warming, higher temperatures would be expected to directly lower oxygen concentrations and enhanced stratification to reduce the flow of well-ventilated surface waters to the interior (Le Quere et al., 2002). Under such circumstances the open-ocean dead zones could greatly expand (Shaffer et al., 2009; Fröhlicher et al., 2009) and indeed changes in low-oxygen waters have been invoked as evidence of climate change (Stramma et al., 2010).

However, recent work (Duteil and Oschlies, 2011) found that suboxia (oxygen less then $0.2\,ml\,l^{-1} \sim 8.8\,\mu M$) did not necessarily increase under global warming. In this paper we use an Earth System Model to demonstrate that this simultaneous increase

Discussion Paper | Discussion Paper | Discussion Paper | Discussion Paper |

BGD

8, 7007–7032, 2011

Will open ocean oxygen stress intensify under climate change?

A. Gnanadesikan et al.

in volume yet decrease in intensity of oceanic hypoxia can be explained by changes in the balance between pathways that connect interior waters to the surface on short and long time scales. Such changes have previously been shown to explain why tropical waters between 300 and 1500 m become younger with respect to exchange with the surface under global warming in coupled models (Gnanadesikan et al., 2007). While the application of this method to oxygen cycling is more complex, the conclusion is similar for the bulk of hypoxic waters. For the suboxic waters of the Southeast Pacific, we show that the changes in ventilation involve a change in convection off the Chilean coast, spurred by changes in the heat and freshwater balance of this region.

2 Methods

The model used in this paper is an implementation of the GFDL physical climate model CM2.1 (Delworth et al., 2006; Gnanadesikan et al., 2006) which was used for the Intergovernmental Panel on Climate Change's Fourth Assessment report (IPCC AR4). This model consists of an approximately 2-degree resolution atmosphere with 24 vertical levels atop an approximately 1-degree resolution ocean with 50 vertical levels and a sea ice model with five thickness classes. Considering metrics of relevance to this paper, CM2.1 generally ranks as one of the most skilful IPCC AR4 models in simulating atmospheric climate (Reichler and Kim, 2006), the El Niño Southern Oscillation cycle (van Oldenborgh et al., 2005) and the hydrography of the Southern Ocean (Russell et al., 2006). It does share with many other climate models a bias towards overly thin stratus decks above upwelling zones, resulting in significant warm biases in sea surface temperatures in these regions.

The Earth System Model 2.1 adopts the parameterizations and settings of CM2.1 for the atmosphere, ocean physics, and sea ice. On the land, the fixed stomatal resistance and albedo used by CM2.1 based on observed land properties is replaced by properties predicted by the LM3v dynamic vegetation model of Shevliakova et al. (2009). Additionally, the absorption of shortwave radiation in CM2.1 is parameterized using a

BGD
8, 7007–7032, 2011

satellite-based chlorophyll, while ESM2.1 uses the chlorophyll predicted by the Tracers of Ocean Productivity with Allometric Zooplankton (TOPAZ) code (Dunne et al., 2010; Gnanadesikan et al., 2011). The net effects of including prognostic ecosystems on ocean circulation are quite minor.

The version of the ocean biogeochemical model TOPAZ used in ESM2.1 resolves three classes of the phytoplankton which sit at the base of the marine food web: small phytoplankton, large phytoplankton, and diazotrophs. Organic material produced by the grazing of phytoplankton is divided into a fraction associated with denser ballast materials (opal, calcium carbonate, and lithogenic material) that remineralizes when these materials dissolve and an unprotected fraction not associated with ballast. The unprotected fraction is remineralized to ammonia with a constant depth scale of $w_{\text{sink}}/R = 180$ m where w_{sink} is the sinking velocity and R is a remineralization rate. Large phytoplankton are associated with more production of organic material associated with ballast and thus protected from rapid remineralization. Highly productive regions thus see more efficient export of organic material from the mixed layer (Dunne et al., 2005).

The remineralization rate R is suppressed in the absence of oxygen:

$$R = \frac{r_{\text{oxic}} \cdot \max(O_2, O_{2\min})}{K_{O_2} + O_2} \tag{1}$$

where O_2 is the oxygen concentration and $K_{O_2} = 20\,\mu M$. This provides for oxygen limitation of oxic respiration down to a minimum value of oxygen ($O_{2\min} = 1\,\mu M$) at which the decay of organic matter switches over to denitrification at the same rate. Equation (1) represents the contrast in oxic- and denitrification-modulated depth scales between the Mexican and Washington Margins as seen by Devol and Hartnett (2001).

Ocean temperature and salinity in ESM2.1 are initialized from the CM2.1 1860 control run after 2000 yr of run. Ocean nutrients in ESM2.1 are initialized from observations and then run with interactive chlorophyll and an interactive land biosphere but with radiatively active gasses fixed at 1860 levels for another 1600 yr. Historical runs with volcanic, aerosol and well-mixed greenhouse gas forcings are then spun off of these simulations and run out to year 2000. At this point, future scenarios are spun off the main branch and run out for another 300 yr. For this paper, we focus on the relatively aggressive A2 scenario (Nakicenovic et al., 2000) in which greenhouse gas levels rise sharply until 2100. After this point we assume stabilization of greenhouse gas levels, so that our simulation exhibits a maximum in radiative imbalance at the top of the atmosphere of about 2.6 W m^{-2} around the year 2100. This is in contrast to Schmittner et al. (2008) who instead prescribe a linear decrease in emissions from 2100 to 2300, resulting in a further increase in greenhouse forcing over this time period.

3 Results

3.1 Control oxygen simulation

At 300 m depth, hypoxic ($O_2 < 2\,\mathrm{ml\,l^{-1}} \sim 88\,\mu\mathrm{M}$; a commonly used definition of where low oxygen concentration start to affect fish) waters are found along the eastern edges of the tropical ocean basins, as well as in the North Pacific and Northern Indian Ocean (Fig. 1a). These regions are unique in being advectively disconnected from regions of deep wintertime convection where oxygenated surface waters are injected into the ocean interior (Luyten et al., 1983; Gnanadesikan et al., 2007). The model is largely able to simulate the pattern of high and low oxygen regions (Fig. 1b), with a correlation of 0.88 at 300 m and 0.83 globally. The model captures the location of the tropical oxygen minimum zones in the eastern basins relatively well with a modeled hypoxic volume of 157 M km^3 comparable to the observed 148 M km^3. However, when suboxia ($O_2 < 0.2\,\mathrm{ml\,l^{-1}} \sim 8.8\,\mu\mathrm{M}$; the realm where bacterial cycling moves to alternative electron receptors such as nitrogen) is considered, the model predicts far too large a volume. This overprediction is largely due to the creation of suboxic waters throughout the water column in the Panama Basin, which appears to be far too isolated in our model. If we focus on depths above 1000 m (where most suboxic waters in the present-day ocean are found) the volume of suboxic waters is within 10 % of a recent synthesis of observations (D. Bianchi, personal communication, 2011).

As noted in Gnanadesikan et al. (2011), the model also does a good job at matching the zonal integral of primary production estimated from satellite as well as the globally averaged vertical profile of oxygen. Besides the Panama basin, the main failure of the model comes from its inability to develop very low oxygen in the North Pacific, a failure associated with excessive production of weakly stratified North Pacific Mode Water to the east of Japan.

Running a dynamical model allows quantification of the various terms that contribute to the oxygen budget, as these terms are separately calculated in the code. As the integrated trend (net change in oxygen concentration) of oxygen below a given depth $T(z)$ (solid black line in Fig. 1c) is essentially zero over the twenty year averaging period considered here, the model oxygen is in approximately steady state.

$T(z)$ must be equal to the sum of four terms.

$$T(z) = S(z) + A(z) + E(z) + D(z) \tag{2}$$

The first of these terms $S(z)$ is the integrated source (production-consumption) of oxygen below depth z. Shown by the dashed black line in Fig. 1c, this term is negative throughout the water column, representing the consumption of oxygen by remineralization of organic matter. This negative term is balanced by a number of supply terms. The red line in Fig. 1c shows supply of oxygen due to advection by the large scale flow that is resolved by the model $A(z)$. The green line in Fig. 1c represents $E(z)$, the total neutral diffusive tendency (Griffies et al., 1998) which parameterizes the transport of oxygen by mesoscale eddies with horizontal scales of tens of km. The blue line shows $D(z)$, the sum of transport by three small-scale diffusive processes including (1) breaking internal waves (as given by the implicit vertical diffusive tendency in the model) (2) convective transport (as given by the convective adjustment tendency that mixes away any cases where dense water overlies light water), and (3) mixed layer eddies (associated with the nonlocal K-profile parameterization transport of Large et al., 1994). As all these fluxes vanish at lateral boundaries, integrating these tendencies in the horizontal and then up from the bottom gives a flux of oxygen at depth z, where a positive value denotes a downward flux. As seen in Fig. 1c, in the upper water column the basic balance is between downward mixing of oxygen and consumption of that oxygen through remineralization. Below about 400 m however, the small-scale mixing drops off sharply and the dominant supply of oxygen to the deep is via advection due to the resolved flow.

3.2 Future changes

The time series of the relative change of global oxygen concentrations show a basically monotonic decrease of 10 % by year 2300 (Fig. 2a, black line). This decline is not just due to warming, as the oxygen saturation (Fig. 2a magenta line, corresponding to the oxygen content in equilibrium with the atmosphere) drops only by around 2.8 %. The volume of hypoxic water grows monotonically by 18 % over this same time period (Fig. 2a, red line). By contrast, the volume of suboxic water experiences a more subtle response to climate change. Similar to the low-diffusivity subset of the Duteil and Oschlies (2011) simulations, our model decreases the volume of suboxic water under global warming in the 21st century. The suboxic water volume reaches a minimum in the 22nd century and starts to rise as CO_2 stabilizes after 2100 (blue line, Fig. 2a). Even at year 2300, the volume of suboxic waters is slightly lower in our climate change case than in our control. Examining the changes in oxygen at 300 m (Fig. 2b) and at 800 m (Fig. 2c) we see that the oxygen levels in the heart of a number of oxygen minimum zones (though most strongly in the Southeast Pacific) are higher at year 2300 than in the control, thus explaining the decline in the suboxic volume. The increase in the Southern Hemisphere also shows up in an east-west average of the oxygen change (Fig. 2d).

The oxygen change can be broken into two components, one due to the change in oxygen solubility (Fig. 3a) and a residual component dominated by changes in biogeochemical cycling (Fig. 3b). In the regions where an increase in oxygen is seen at year

BGD
8, 7007–7032, 2011

2300 the dominant term is this second, primarily biological, component. Below the euphotic zone, an increase in the oxygen field associated with biogeochemical cycling is likely to be the result of one of two mechanisms, a decrease in the rate at which oxygen is consumed by remineralization, or a decrease in the average time required for waters to travel from the surface to the region – the ventilation time. A decrease in the ventilation time would mean that waters would have less time to accumulate an oxygen deficit.

The average ventilation time can be estimated using a tracer known as ideal age, which is set to zero in the surface layer and ages at a rate of $1\,\mathrm{yr\,yr^{-1}}$ below that. Contours of the ideal age change under global warming are plotted over the residual age change in Fig. 3b, illustrating that zero contours for the two fields largely overlie each other. A scatterplot of oxygen change vs. age change (Fig. 3c) also shows a strong relationship between the two. Regions that are getting older have decreased oxygen while regions getting younger have increased oxygen. Ideal age decreases in the mid-depth tropics have been seen in a number of climate models (Bryan et al., 2006; Gnanadesikan et al., 2007; Duteil and Oschlies, 2011), even though these models predict an overall slowdown in the ocean overturning circulation. The reason is that the age of water at a given point represents an integral over a large number of pathways from the surface. Some of these pathways are relatively direct and require less time while some, generally associated with upwelling of deep water, require hundreds or even thousands of years to travel from the surface to a particular point.

As shown in previous work, under global warming the balance at mid-depths shifts towards the short-time pathways associated with the subtropical gyres (red dots, Fig. 3c) and away from the long-time pathways associated with deep overturning in the Southern Ocean – which shows a much larger increase in age (blue dots, Fig. 3c). This disproportionate sensitivity of the deep Southern Ocean overturning to warming and freshening results from the strong dependence of stratification in this region on the hydrological cycle.

BGD
8, 7007–7032, 2011

The reverse of this picture is seen in the North Pacific, where there is a decrease in the oxygen (Fig. 2b) associated with biological cycling (Fig. 3b) and associated with an increase in the age locally. As discussed by Rykaczewski and Dunne (2010) the increase in age is largely the result of a shift of the convective area supplying these waters westward, resulting in an increase in the transit time of waters from the convective outcrop to the boundary regions, allowing more time for oxygen to be drawn down. Additionally, a sharp increase in the upwelling nitrate concentration leads to an increase in the local consumption of oxygen beneath the coastal upwelling.

On a global scale, changes in the supply terms show a complicated picture. At depth, the integrated trend in oxygen burden $T(z)$ (solid black line) becomes more negative as one moves up into the water column from the bottom, corresponding to a lowering of oxygen concentration. At the base of the thermocline (about 700 m), however, this line becomes more or less constant with depth, so that oxygen levels are no longer decreasing at these levels. Changes to the advective supply of oxygen $A(z)$ match up well with the deep trend in terms of pattern and magnitude below 2000 m, explaining almost all of the change. Between 2000 and 700 m however, we see that the advective supply curve starts to move to the right. This pattern means that the net advective tendencies at these depths are positive because advection is causing the waters to become more oxygenated. As noted in Gnanadesikan et al. (2007) this is also the pattern of change seen for age. The diffusive supply grows steadily more negative through most of the water column, so that small-scale diffusion is generally causing the waters to become less oxygenated as expected.

By contrast, changes in the biological consumption of oxygen $S(z)$ (dashed black line) are generally positive, so that biological cycling is acting to make the deep ocean more oxygenated. The reduction in deep upwelling in the tropics and reduction of small-scale mixing due to stratification in high latitudes reduces the supply of nutrients to the surface ocean and reduces the globally averaged rates of biological productivity (Steinacher et al., 2009). This in turn reduces oxygen consumption in the deep ocean. In a global sense then, while advection is most qualitatively consistent with negative changes in oxygen at depth and positive changes at mid-depth, diffusion and production also play key roles in the overall balance.

Limiting our analysis to the region from 40° S to 5° N and 300 to 1500 m, we examine the change in the budget terms for trend, large scale advection, small-scale diffusion, mesoscale eddies and source. As seen in Table 1, when these terms are normalized by the biological consumption of oxygen in the control run, we see that in the there is initially a small negative trend in oxygen (1.3 % of the oxygen consumption). This trend arises because advection, small-scale diffusion and mesoscale eddies together balance 98.7 % of the source over this volume, with advection accounting for the bulk of the supply. Under global warming, the trend switches sign, so that oxygen actually increases. This increase arises because there is less oxygen consumption and more advective supply in these waters. In contrast, both the small-scale diffusive supply and mesoscale eddy supply drop sharply. The fact that advection supplies more oxygen but not more nutrients to drive higher consumption is consistent with the picture seen in the global average budget (Fig. 3d) and with the previous analysis for ideal age, with more influence from high-oxygen, low-nutrient, young surface waters and less from the older deep waters that carry higher values nutrients along with oxygen.

Limiting ourselves yet further to suboxic zones between 300 and 1500 m in the Southern Hemisphere (3rd and 4th lines, Table 1) gives a different sense of the important balances. First, the dominant supply of oxygen to these regions is the mesoscale eddy term, which accounts for more than 80 % of the oxygen consumption of 9.7 Tmol yr^{-1} in the control run. Isopycnal diffusion is much more important in these relatively stagnant regions that are isolated from surface outcrops (Luyten et al., 1983). This fact highlights the importance of properly constraining isopycnal diffusive processes in such regions. Additionally, the sensitivity of remineralization to global warming is very different for the suboxic fraction of this volume compared with the volume as a whole. Oxygen consumption actually rises by 28.7 % under global warming. This rise is a consequence of rising oxygen levels. As expected from Eq. (2) higher oxygen concentrations allow for higher rates of remineralization in the suboxic zone.

Such a rise in remineralization rate may be a model artifact as the suppression of the remineralization rate in the Control model results in spreading the oxygen minimum zones excessively in the vertical.

The reason that the rise in oxygen consumption does not result in a decrease in oxygen concentration is that the mesoscale eddy supply of oxygen jumps by 2.5 Tmol yr^{-1} and the small-scale diffusive supply almost doubles, increasing by 0.7 Tmol yr^{-1}. These increases compensate both the increase in consumption and a small decrease in advective supply.

Focusing on the mesoscale eddy source within the suboxic zone, we see the biggest impacts off the Chilean coast. The change in averaged oxygen concentration (contours, Fig. 4a) between 300 and 500 m in this region shows a plume of higher oxygen emanating from the Chilean coast, and hugging the edge of the oxygen minimum zone. Away from the Chilean coast, this increase is associated with an increase in the advective tendency (not shown). The integrated mesoscale eddy tendency (colors, Fig. 4a) acts to smooth out this change, with negative values in the center of the plume of higher oxygen and positive values on the edges. Positive values of mesoscale eddy oxygen tendency on the equatorward side of the plume correspond to the increased oxygen supply to the suboxic zones seen in Table 1.

The source of the oxygen off the Chilean coast is deepening wintertime convection in the region from 39° S to 33° S and 76° S to 72° W outlined by the box in Fig. 4a. As seen in Fig. 4b, all three vertical mixing terms increase sharply in this region under global warming, with convection (black line) and nonlocal mixing associated the K-Profile Parameterization (blue line) dominating in the upper 200 m, but with some signal seen down to 500 m (indicating that at some point during the 20 yr time period the mixed layer penetrates to these depths). Below about 200 m, however, the dominant term supplying higher oxygen to depth is the small-scale vertical diffusion associated with breaking internal waves (blue line), so that there is usually a "handoff" between mixed layer and interior processes between 200 and 300 m.

BGD
8, 7007–7032, 2011

Will open ocean oxygen stress intensify under climate change?

A. Gnanadesikan et al.

Although the term balances are more sensitive diagnostics of mixed layer processes, the change in mixed layer depth is seen in the climatology as well. Figure 5a shows the maximum monthly climatological boundary layer depths (as calculated from the KPP mixed layer code) off South America for the Control model. These depths represent the average depth to which active mixing occurs over one month. Note that the boundary layers do have a local maximum off of central Chile, even in this simulation, but that it only penetrates to around 65 m, in rough agreement with observations of the region (Silva and Guzman, 2006; Sobarzo et al., 2007).

The annually integrated buoyancy flux ΔB can be calculated as

$$\Delta B = \int \left(-\frac{g\alpha Q}{\rho c_p} + g\beta S F_\mathrm{w} \right) dt \equiv \Delta B_T + \Delta B_S \tag{3}$$

where g is the gravitational acceleration, α is the coefficient of thermal expansion, Q is the surface heat flux, ρ is the density of seawater, c_p is the specific heat, β is the coefficient of haline contraction, S is the salinity, F_w is the freshwater flux and an integral is taken over the entire year. ΔB_T and ΔB_S can then be defined as the thermal and haline components of ΔB, corresponding to the first and second terms under the integral. In the Control simulation, the Central Chilean coast is a region of positive buoyancy flux, as are the very shallow mixed layers further to the north.

In the A2 scenario, by contrast (Fig. 5b), the boundary layer depth off Chile reaches 290 m and mixed layer depths (defined using a density criterion as in global climatologies) reach 440 m or more at individual grid points. While such deep mixed layers may seem surprising, the modern ARGO-based climatology of Holte et al. (2010) does show maximum mixed layer depths exceeding 200 m over large parts of the Southeast Pacific during Austral winter in regions which in the Control model are associated with annual-mean buoyancy loss. Under global warming the Central Chilean coast also becomes a region with negative ΔB, so that surface fluxes act to make the waters denser.

The contributors to ΔB in the control region 39–33° S, 76–72° W off the Central Chilean coast are analyzed in Fig. 5c, which shows cumulative fluxes integrated

BGD
8, 7007–7032, 2011

Will open ocean oxygen stress intensify under climate change?

A. Gnanadesikan et al.

through the year and Table 2, which breaks down the annual mean contributors to the heat and freshwater fluxes. In the Control, the wintertime cooling is much less than the summertime warming and the freshwater balance is near neutral with significant runoff in the autumn and winter. Both the net heating over the year and freshening during winter help to limit the penetration of convection in the model as in the real world (Sobarzo et al., 2007). Under global warming, the heat balance becomes slightly negative during the year, switching sign from +30 to $-9\,\mathrm{W\,m^{-2}}$. This change is largely the result of an increase in evaporative cooling during the wintertime. Additionally, the freshwater balance becomes negative throughout the season, so that the hydrological cycle acts to make surface waters much denser. The net freshwater flux in the control region drops by more than $1\,\mathrm{m\,yr^{-1}}$. This is one of the largest declines in freshwater supply seen in mid-latitudes under global warming. About half of the drop is due to increased evaporation, while the remainder is due to a 75 % reduction in runoff and a decline in in-situ precipitation. On a seasonal scale, the heat fluxes have the biggest impact on the buoyancy fluxes, but when the integral over the entire year is taken, the freshwater fluxes play the dominant role in the net extraction of buoyancy from this region.

The impact of the reduced freshwater flux can be seen in a T-S plot of the region (Fig. 5d). In the Control simulation surface waters (black points) are always much fresher and lighter than waters at 200 m (red points), with a difference quite similar to that seen in observations. Under global warming the surface waters (blue points) become much saltier. This increasing salinification brings the surface waters much closer to the waters at 200 m (magenta points) and preconditions the column for wintertime convection. The T-S plot off central Chile under global warming is much more like the modern ocean off of Southeast Australia, where deep mixed layers are currently seen in salty, subtropical waters (Holte et al., 2010).

These changes in heat and freshwater balance reflect larger-scale changes in the atmospheric circulation over the Southeast Pacific. As shown in Fig. 6a, under global warming in CM2.1 the subtropical high over the Southeast Pacific strengthens and

BGD
8, 7007–7032, 2011

the winds over central Chile shift from being off the ocean to more along the coast. As a result, less moisture is brought into this region, resulting in a sharp decline in precipitation (Fig. 6b) and a significant drop in relative humidity of up to 13 % (Fig. 6c). While the CM2.1 model is somewhat extreme in its prediction of such large precipitation changes, most of the IPCC AR4 models examined by Vera et al. (2007) show drying in this region, with all seven models showing drying during the high-precipitation period of April–June. The drop in relative humidity then results in much higher evaporation and latent cooling of the ocean (Fig. 6d and Table 2).

4 Discussion and conclusions

We have shown that oxygen concentrations exhibit a complicated response to climate change linked to circulation. On a broad scale, these changes are linked to changes in the advective flux of older deep waters into intermediate depths. Within suboxic zones such as that off South America, however, changes in convection and vertical mixing associated with salinification of the surface produce a pool of more oxygenated water. This water is advected along the edge of the oxygen minimum zone and diffused by isopycnal mixing into the suboxic zone. This suggests that the simulated changes in the volume of suboxic water can depend sensitively on local changes in heat and salt, as well as on the representation of isopycnal diffusivity. While the isopycnal tracer diffusion coefficient (as opposed to the layer thickness diffusion coefficient) has been found to have a relatively minor impact on the circulation within our coupled models our results suggest that it has a big impact on the degree of suboxia that develops within the tropics. The isopycnal tracer diffusion coefficient in ESM2.1 is set to a relatively large spatially and temporally constant value of 600 $m^2 s^{-1}$ (Gnanadesikan et al., 2006). We would expect that models with lower values than this would have trouble with suboxia. Additionally, our results suggest that simplified advection-diffusion models should be used with caution in projecting the behavior of suboxic waters into the future, as such models are unlikely to capture the details of ventilation of these rather special locations.

BGD
8, 7007–7032, 2011

Our results also suggest that recent attribution of increases in the volume of hypoxic waters may depend strongly on the cutoff used. Hypoxia associated with fish (a relatively high oxygen threshold) would be expected to increase under global warming. However, if local increases in suboxia (with a relatively low oxygen threshold) are observed in the next few decades, explanations for such changes should be sought in long-period climate variability as well as secular changes associated with global warming. Conversely, if oxygen concentrations were found to increase in the suboxic oxygen minimum zones, such increases would be consistent with global warming even as oxygen in the broader ocean decreases.

The prediction that warming does not necessarily lead to increased suboxic volume should not be extrapolated to all climates. As our simulations focus on a few centuries of warming and on the open ocean, they are not inconsistent with suboxia developing over time scales of many centuries in the deep ocean or over shorter periods in coastal waters. Given increasing evidence that the much of the impact of greenhouse gas emissions will persist for millennia (Schmittner et al., 2008) this possibility deserves further study. Our results also suggest that a reinvigorated ocean overturning circulation could increase suboxia as deep, low-oxygen waters are advected into the oxygen minimum zones.

Finally, it should be acknowledged that modelled increases in mid-depth oxygen in the current generation of earth system models may reflect some common failings in model formulation. These failings may be related to representation of physical modes of ventilation and overly simplistic representation of how biology sets the regional pattern and depth scale of remineralization. Resolving this issue is of critical importance for understanding the potential impacts of climate change on interior ocean habitat for fish and ocean biogeochemical cycles, particularly in the light of paleoclimatic results suggesting that anoxic events associated with global warming could have caused mass extinctions such as that at the end of the Permian (e.g. Wignall and Twichett, 1996).

Acknowledgements. We thank Ryan Rykaczewski, Daniele Bianchi, Jorge Sarmiento and Thomas Frölicher for useful discussions and comments on this manuscript.

BGD

8, 7007–7032, 2011

Will open ocean oxygen stress intensify under climate change?

A. Gnanadesikan et al.

References

Bryan, F. O., Danabasoglu, G., Gent, P. R., and Lindsay, K.: Changes in ocean ventilation during the 21st century in the CCSM3, Ocean Model., 15, 141–156, 2006.

Delworth, T. L., Broccoli, A. J., Rosati, A., Stouffer, R. J., Balaji, V., Beesley, J. A., Cooke, W. F., Dixon, K. W., Dunne, J., Dunne, K. A., Durachta, J. W., Findell, K. L., Ginoux, P., Gnanadesikan, A., Gordon, C. T., Griffies, S. M., Gudgel, R., Harrison, M. J., Held, I. M., Hemler, R. S., Horowitz, L. W., Klein, S. A., Knutson, T. R., Kushner, P. J., Langenhorst, A. R., Lee, H.-C., Lin, S.-J., Lu, J., Malyshev, S. L., Milly, P. C. D., Ramaswamy, V., Russell, J., Schwartzkopf, M. D., Shevliakova, E., Sirutis, J. J., Spelman, M. J., Stern, W. F., Winton, M., Wittenberg, A. T., Wyman, B., Zeng, F., and Zhang, R.: GFDL's CM2 global coupled climate models – Part 1: Formulation and simulation characteristics, J. Climate, 19, 643–674, 2006.

Devol, A. H. and Hartnett, H. E.: Role of the oxygen-deficient zone in transfer of organic carbon to the deep ocean, Limnol. Oceanogr., 46, 1684–1690, 2001.

Dunne, J. P., Armstrong, R. A., Gnanadesikan, A., and Sarmiento, J. L.: Empirical and mechanistic models of particle export, Global Biogeochem. Cy., 19, GB4026, doi:10.1029/2004GB002390, 2005.

Dunne, J. P., Gnanadesikan, A., Sarmiento, J. L., and Slater, R. D: Technical description of the prototype version (v0) of Tracers of Phytoplankton with Allometric Zooplankton (TOPAZ) ocean biogeochemical model as used in the Princeton IFMIP model, Biogeosciences, 7, 3593, Supplement, available at: http://www.biogeosciences.net/7/3593/2010/bg-7-3593-2010-supplement.pdf, 2010.

Duteil, O. and Oschlies, A.: Sensitivity of simulated extent and future evolution of marine suboxia to mixing intensity, Geophys. Res. Lett, 38, L06607, doi:10.1029/2011GL046877, 2011.

Frölicher, T., Joos, F., Plattner, G.-K., Steinacher, M., and Doney, S. C.: Natural variability and anthropogenic trends in oceanic oxygen in a coupled carbon-cycle climate model ensemble, Global Biogeochem. Cy., 23, GB1003, doi:10.1029/2008GB003316, 2009.

Garcia, H. E., Locarnini, R. A., Boyer, T. P., Antonov, J. I., Baranova, O. K., Zweng, M. M., and Johnson, D. R.: Dissolved Oxygen, Apparent Oxygen Utilization and Oxygen Saturation, in: World Ocean Atlas 2009 Volume 3, edited by: Levitus, S., NOAA Atlas, NESDIS 70, U.S. Government Printing Office, Washington, D.C., 344 pp., 2010.

Gnanadesikan, A., Dixon, K. W., Griffies, S. M., Balaji, V., Barreiro, M., Beesley, J. A., Cooke, W. F., Delworth, T. L., Gerdes, R., Harrison, M. J., Held, I. M., Hurlin, W. J., Lee, H. C., Liang, Z., Nong, G., Pacanowski, R. C., Rosati, A., Russell, J. L., Spelman, M., Samuels, B. L., Song, Q., Spelman, M. J., Stouffer, R. J., Sweeney, C., Vecchi, G., Winton, M., Wittenberg, A., Zeng, F., Zhang, R., and Dunne, J. P.: GFDL's CM2 global coupled climate models – Part 2: The baseline ocean simulation, J. Climate, 19, 675–697, 2006.

Gnanadesikan, A., Russell, J. L., and Fanrong Zeng: How does ocean ventilation change under global warming?, Ocean Sci., 3, 43–53, doi:10.5194/os-3-43-2007, 2007.

Gnanadesikan, A., Dunne, J. P., and John, J.: What ocean biogeochemical models can tell us about bottom-up control of ecosystem variability, ICES J. Mar. Sci., 68, 1030–1044, doi:10.1093/icesjms/fsr068, 2011.

Griffies, S. M., Gnanadesikan, A., Pacanowski, R. C., Larichev, V. D., Dukowicz, J. K., and Smith, R. D.: Isoneutral diffusion in a z-coordinate ocean model, J. Phys. Oceanogr., 28, 805–830, 1998.

Holte, J., Gilson, J., Talley, L., and Roemmich, D.: Argo Mixed Layers, Scripps Institution of Oceanography/UCSD, http://mixedlayer.ucsd.edu, access: 22 June 2011, 2010.

Large, W. G., McWilliams, J. C., and Doney, S. C.: Oceanic vertical mixing: a review and a model with a non-local K-profile boundary layer parameterization, Rev. Geophys., 32, 363–403, 1994.

Le Quere, C., Heimann, M., Manning, A. C., and Monfray, P.: Climate-induced oceanic oxygen fluxes: Implications for the contemporary carbon budget, Global Biogeochem. Cy., 16, 1022, doi:10.1029/2001GB001445, 2002.

Luyten, J. L, Pedlosky, J., and Stommel, H. M.: The ventilated thermocline, J. Phys. Oceanogr., 13, 292–309, 1983.

Nakicenovic, N., Alcamo, J., Davis, G., de Vries, B., Fenhann, J., Gaffin, S., Gregory, K., Grübler, A., Jung, T. Y., Kram, T., La Rovere, E. L., Michaelis, L., Mori, S., Morita, T., Pepper, W., Pitcher, H., Price, L., Riahi, K., Roehrl, A., Rogner, H.-H., Sankovski, A., Schlesinger, M., Shukla, P., Smith, S., Swart, R., van Rooijen, S., Victor, N., and Dadi, Z.: Emissions Scenarios, Special Report, Working Group III, Intergovernmental Panel on Climate Change, Cambridge Univ. Press, Cambridge, 2000.

Reichler, T. and Kim, J.: How well do coupled climate models simulate today's climate?, B. Am. Meteorol. Soc., 89, 303–311, 2008.

Russell, J. L., Stouffer, R. J., and Dixon, K. W: Intercomparison of the Southern Ocean Circulations in IPCC Coupled Model Control Simulations, J. Climate, 19(18), 4560–4575, doi:10.1175/JCLI3869.1, 2006.

BGD
8, 7007–7032, 2011

Will open ocean oxygen stress intensify under climate change?

A. Gnanadesikan et al.

Rykaczewski, R. and Dunne, J. P.: Enhanced nutrient supply to the California Current Ecosystem with global warming and increased stratification in an earth system model, Geophys. Res. Lett., 37, L21606, doi:10.1029/2010GL045019, 2010.
Schmittner, A., Oschlies, A., Matthews, H. D., and Galbraith, E. D.: Future changes in climate, ocean circulation, ecosystems and biogeochemical cycling simulated for a business-as-usual CO_2 emission scenario until year 4000 AD, Global Biogeochem. Cy., 22, GB1013, doi:10.1029/2007GB002953, 2008.
Shaffer, G., Olsen, S. M., and Pedersen, J. O. P.: Long-term ocean oxygen depletion in response to carbon dioxide emissions from fossil fuels, Nat. Geosci., 2, 102–105, 2009.
Shevliakova, E., Pacala, S. W., Malyshev, S., Hurtt, G. C., Milly, P. C. D., Caspersen, J. P., Sentman, L. T., Fisk, J. P, Wirth, C., and Crevoisier, C.: Carbon Cycling Under 300 Years of Land-Use Change: The Importance of the Secondary Vegetation Sink, Global Biogeochem. Cy., 23, GB2022, doi:10.1029/2007GB003176, 2009.
Silva, N. and Guzman, D.: Condiciones oceanographicas fisicas y quimicas entre Boca del Guafo y Fiordo Aysen (Crucero CIMAR 7 Fiordos), Cienc. Tecnol. del Mar, 29, 24–44, 2006.
Sobarzo, M., Bravo, L., Donoso, D., Garcés-Vargas, J., and Schneider, W.: Coastal upwelling and seasonal cycles that influence the water column over the continental shelf off central Chile, Prog. Oceanogr., 75(3), 363–382, 2007.
Stramma, L., Schmidtko, S., Levin, L. A., and Johnson, G. C.: Ocean oxygen minima expansions and their biological impacts, Deep-Sea Res. Pt. I, 57, 587–595, 2010.
Steinacher, M., Joos, F., Frölicher, T. L., Bopp, L., Cadule, P., Cocco, V., Doney, S. C., Gehlen, M., Lindsay, K., Moore, J. K., Schneider, B., and Segschneider, J.: Projected 21st century decrease in marine productivity: a multi-model analysis, Biogeosciences, 7, 979–1005, doi:10.5194/bg-7-979-2010, 2010.
van Oldenborgh, G. J., Philip, S. Y., and Collins, M: El Niño in a changing climate: a multi-model study, Ocean Sci., 1, 81–95, doi:10.5194/os-1-81-2005, 2005.
Vera, C. M., Silvestri, G., Liebmann, B., and Gonzalez, P.: Climate change scenarios for regional precipitation in South America, Geophys. Res. Lett., 33, L13707, doi:10.1029/2006GL025759, 2007.
Wignall, P. B. and Twichett, R. J.: Oceanic anoxia and the End Permian mass extinction, Science, 272, 155–1158, 1996.

BGD
8, 7007–7032, 2011

Will open ocean oxygen stress intensify under climate change?

A. Gnanadesikan et al.

Table 1. Oxygen budget for the region 40° S–5° N, 300–1500 m that shows an increase in oxygen concentration in Fig. 2. All terms are given as a percentage of the oxygen consumption over the relevant volume in the control run.

	Source	Trend	Advection	Small-scale mixing	Mesoscale eddy transport
Control: All waters	100	−1.3	63.8	22.5	12.5
A2: All waters	91.3	0.4	77.7	10.4	3.6
Control: Suboxic	100	−0.5	10.4	8.1	81.9
A2: Suboxic	128.7	0.9	7.3	15.3	107.0

BGD
8, 7007–7032, 2011

Table 2. Annual mean heat, annually integrated water, and annual integrated buoyancy fluxes off Central Chilean coast (76° W–72° W, 39° S–33° S). Heat fluxes in $W\,m^{-2}$, water fluxes in m, and integrated buoyancy fluxes in $m^2\,s^{-2}$.

	1860 Control	A2
Net Shortwave	199	214
Net Longwave	−78	−84
Sensible heat flux	−13	−16
Latent heat flux	−80	−123
Total heat flux	30	−9
Precipitation	0.51	0.32
Runoff	0.37	0.08
Evaporation	1.00	1.55
Total water flux	−0.11	−1.15
Integrated buoyancy flux from temperature	0.55	−0.12
Integrated buoyancy flux from freshwater forcing	−0.03	−0.30
Integrated buoyancy flux	0.52	−0.43

BGD
8, 7007–7032, 2011

Will open ocean oxygen stress intensify under climate change?

A. Gnanadesikan et al.

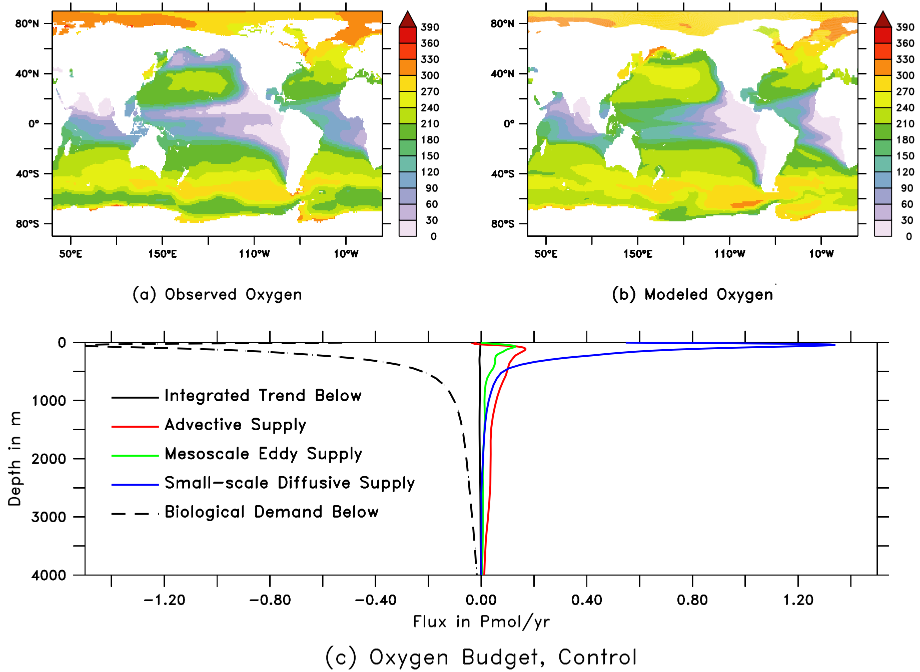

Fig. 1. Current oxygen distribution and budget. **(a)** Observed oxygen in µM at 300 m. **(b)** Modeled oxygen in µM at 300 m. **(c)** Vertically resolved budget of oxygen in 1860 Control simulation. Solid black line is the integrated trend of oxygen below a given depth-near-zero values show that the model is essentially in steady state. Red line, green and blue lines show the supply of oxygen to deeper waters (corresponding to the downward flux) associated with advection, mesoscale eddy fluxes, and small-scale diffusion respectively. Dashed black line shows the net biological source/sink of oxygen below a given depth. The sum of the supply lines and source equals the trend.

BGD
8, 7007–7032, 2011

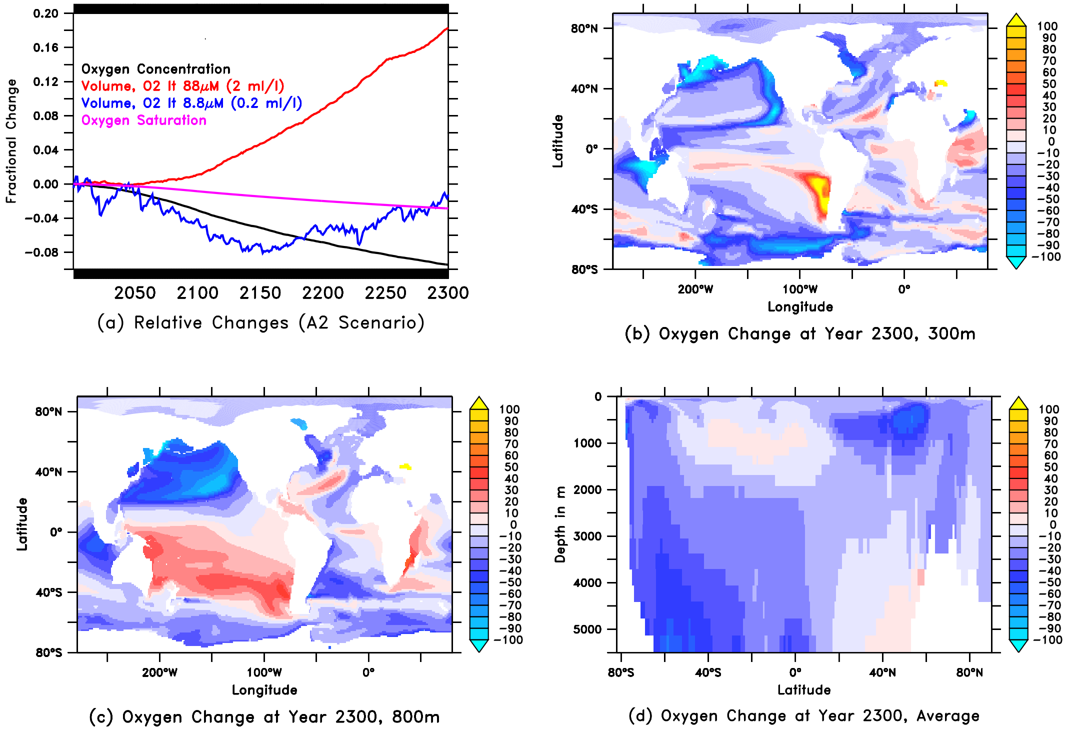

Fig. 2. Oxygen changes under the A2 scenario relative to the control. **(a)** Relative changes in O_2 inventory (black line), volume of hypoxic water (red line) and volume of suboxic water (blue line). **(b)** Oxygen change (mmol m^{-3}) at 300 m depth at year 2300 between A2 run and 1860 control. **(c)** Oxygen change (mmol m^{-3}) at 800 m depth at year 2300 between A2 run and 1860 control. **(d)** Zonally averaged oxygen change (mmol m^{-3}) at year 2300 between A2 run and 1860 control.

BGD

8, 7007–7032, 2011

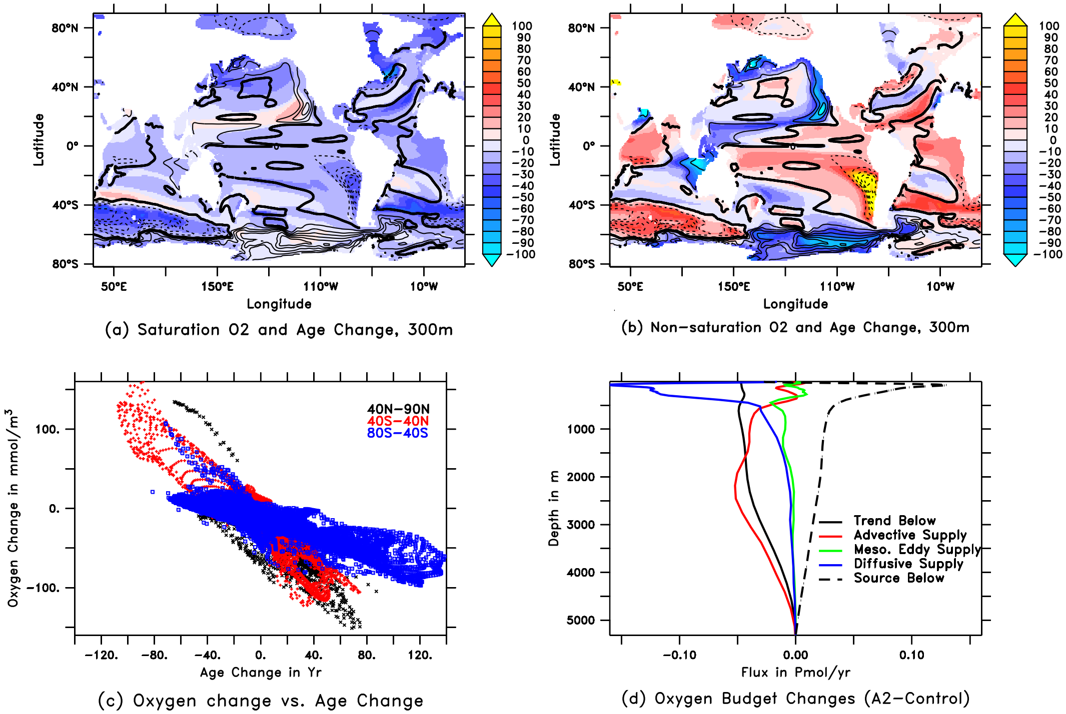

Fig. 3. **(a)** Change in the oxygen saturation at 300 m at 2300 under the A2 scenario, primarily due to change in temperature. Contours of the change in ideal age in years are overlaid (dashed contours negative, solid contours positive, bold contour zero line, contour interval = 20 yr). **(b)** Change in the oxygen concentration at 300 m at year 300 with oxygen saturation effects removed and ideal age change overlaid. Note the correspondence between regions that are getting older/younger and less/more oxygenated. **(c)** Scatterplot of oxygen change vs. age change. **(d)** Change in the oxygen budget.

BGD

8, 7007–7032, 2011

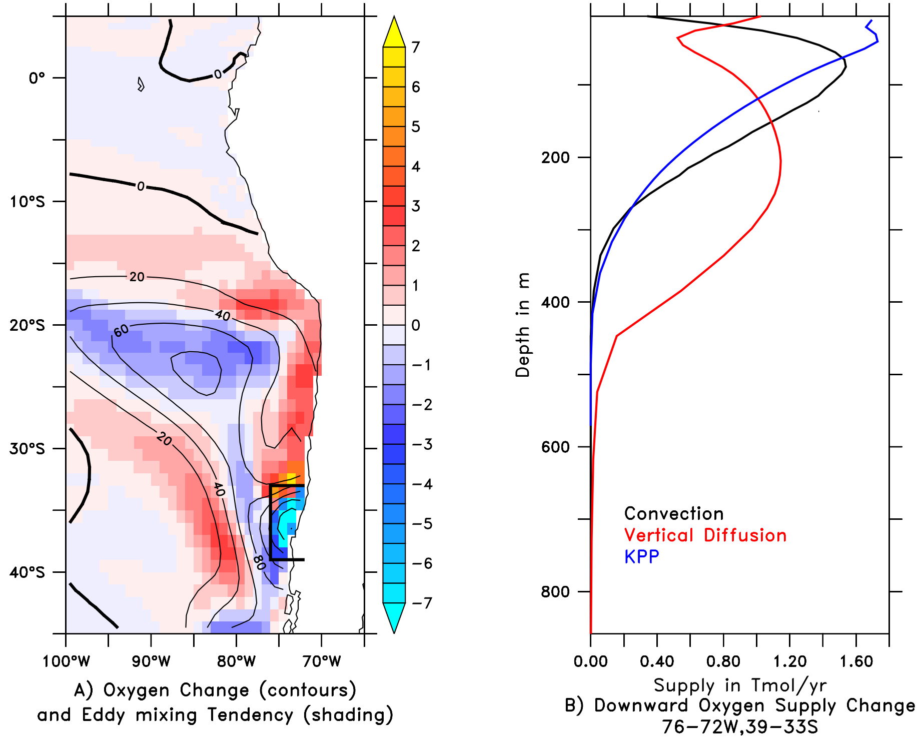

Fig. 4. Oxygen changes in the Southeast Pacific. **(A)** Contours: oxygen change in µM between the A2 and Control runs averaged over 300–500 m. Shading: change in oxygen flux due to mesoscale eddy mixing in mol m^{-2} yr^{-1}. Black lines outline region between 76° W and 72° W, 39° S and 33° S. **(B)** Change in downward flux of oxygen due to diffusive processes integrated over 76–72° W, 39–33° S.

BGD
8, 7007–7032, 2011

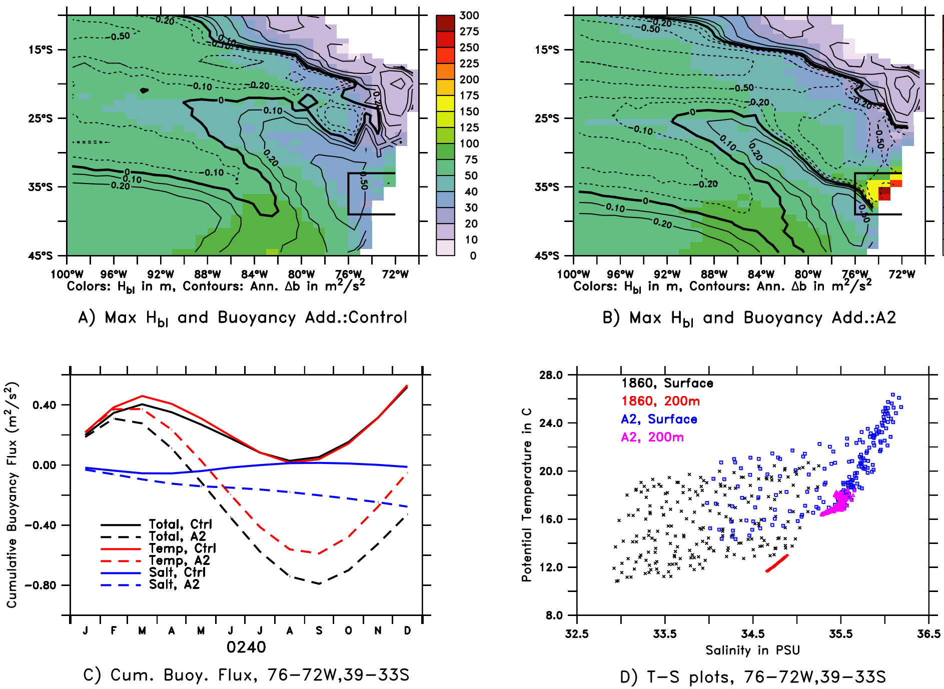

Fig. 5. Physical mechanisms behind increased oxygen supply to the Southeast Pacific. **(A)** Maximum monthly-averaged boundary layer depth in m (depth of active mixing from KPP code) and annually integrated buoyancy flux ΔB in m^2 s^{-2} (Eq. 3) in 1860 Control. Contours are at 0, ±0.1, ±0.2, ±0.5, ±1 and ±2. **(B)** Maximum monthly-averaged boundary layer depth and ΔB in A2 run, contours as in **(A)**. **(C)** Cumulative buoyancy flux from 76° W–72° W, 39° S–33° S. Total is shown in black, contribution from temperature in red, and contribution from salinity in blue. Control runs are solid lines, while A2 is dashed. **(D)** Monthly T-S plots for all ocean grid points between 76° W–72° W, 39° S–33° S. Black symbols show surface points and red symbols 200 m points for Control. Blue symbols show surface points and purple points show 200 m for A2 model.

BGD

8, 7007–7032, 2011

Title Page
Abstract | Introduction
Conclusions | References
Tables | Figures
◀| |▶
◀ ▶
Back | Close
Full Screen / Esc
Printer-friendly Version
Interactive Discussion

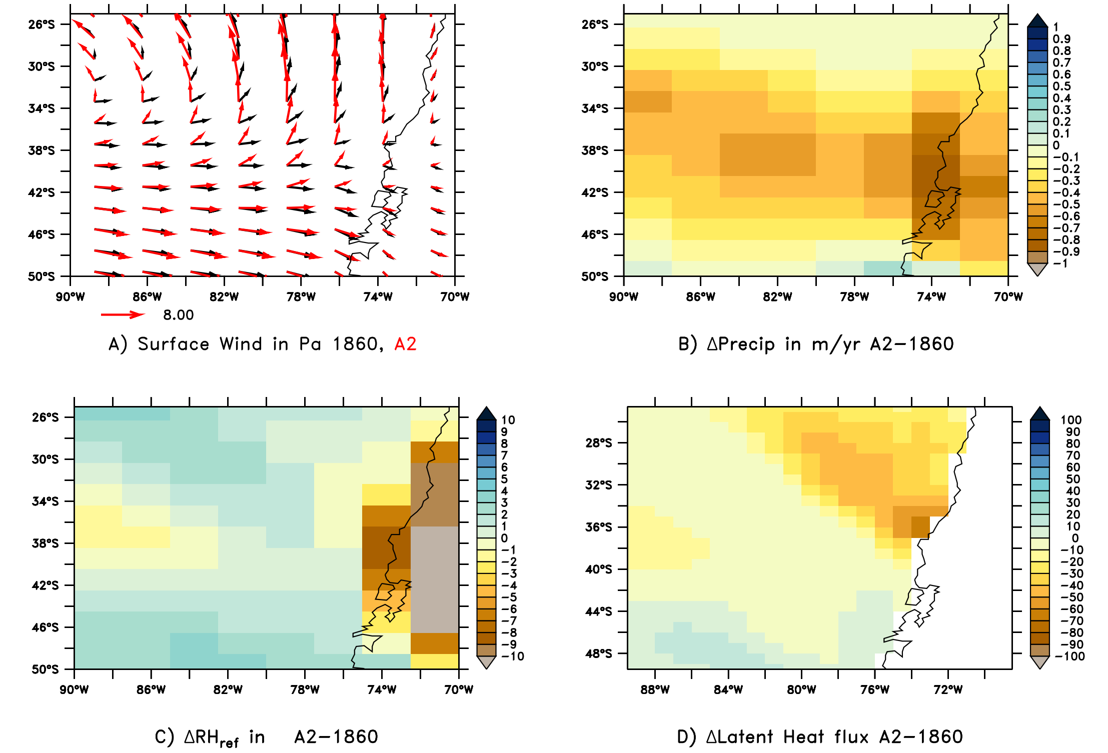

Fig. 6. Atmospheric changes under global warming in the Southeast Pacific. **(A)** Annual-mean surface winds for 1860 control (black) and A2 scenario (red). **(B)** Change in precipitation in $\mathrm{m\,yr^{-1}}$. **(C)** Change in relative humidity in %. **(D)** Change in latent heat flux (negative is loss from ocean) in $\mathrm{W\,m^{-2}}$.

BGD
8, 7007–7032, 2011